Visible light laser guidestar experimental system (Villages): on-sky tests of new technologies for visible wavelength all-sky coverage adaptive optics systems

Donald Gavel*[a], Mark Ammons, Brian Bauman[b], Daren Dillon[a], Elinor Gates[a], Bryant Grigsby[a], Jess Johnson[a], Chris Lockwood[a], Kathleen Morzinski[a], David Palmer[b], Marc Reinig[a], Scott Severson[c],
[a]UCO/Lick Observatory, University of California, Santa Cruz, 95060; [b]Lawrence Livermore National Laboratory, 800 East Ave., Livermore, CA 94550; [c]Department of Physics and Astronomy, Sonoma State University, Rohnert Park, CA 94928

ABSTRACT

The Lick Observatory is pursuing new technologies for adaptive optics that will enable feasible low cost laser guidestar systems for visible wavelength astronomy. The Villages system, commissioned at the 40 inch Nickel Telescope this past Fall, serves as an on-sky testbed for new deformable mirror technology (high-actuator count MEMS devices), open-loop wavefront sensing and control, pyramid wavefront sensing, and laser uplink correction. We describe the goals of our experiments and present the early on-sky results of AO closed-loop and open-loop operation. We will also report on our plans for on-sky tests of the direct-phase measuring pyramid-lenslet wavefront sensor and plans for installing a laser guidestar system.

Keywords: Visible AO, MEMS, Pyramid Sensor, Open Loop Control, MOAO, Laser Guidestar, Laser Uplink

1. INTRODUCTION

Lick Observatory has been a pioneer in the use of adaptive optics for astronomical science since 1994 when a laser guidestar projector was installed at the Lick 3-meter Shane telescope on Mt. Hamilton. In 2000 the Keck Observatory (of which UCO/Lick is a partner) commissioned an AO system of a similar type and by 2004 began science observing with a laser guidestar. In 2003, the Laboratory for Adaptive Optics was established at UC Santa Cruz with a generous grant from the Gordon and Betty Moore Foundation with the purpose of pursuing new ideas in adaptive optics technology. New technologies under investigation include micro-electro-mechanical systems (MEMS) deformable mirrors, precision wavefront sensors, and tomographic methods for wide-field AO systems. The natural extension of the laboratory work is to prove systems on sky using the available observatory facilities on Mt. Hamilton.

We have constructed an experimental visible light adaptive optics system for use on the 1 meter Nickel telescope with the goal of testing MEMS deformable mirrors and other new AO technologies. The MEMS-AO/Visible Light Laser Guidestar Experiments (Villages) project has two phases, the first concentrating on MEMS technology and the second on uplink laser guidestar correction. There are two demonstration milestones in the first phase: 1) that the use of a MEMS deformable mirror is practical in a conventional closed loop AO system in the observatory operating environment and 2) that a MEMS device can be used reliably as an open-loop, or "go-to" wavefront corrector. The later test is an important confidence builder for proposed new architectures in wide field AO systems involving arrangements where the laser guidestar light is sensed ahead of the deformable mirror, such as in a Multi-Object AO (MOAO) arrangement. In brief summary, we have achieved these two milestones during this past year's experiments (October 2007 through April 2008).

In the second phase of Villages, a sodium layer laser guidestar will be installed, along with an uplink AO controller, and a means for launching the beam from the primary mirror of the Nickel telescope. The goal is to demonstrate that uplink correction produces a smaller laser guidestar spot than current laser guidestar systems. Reducing the spot size on the sodium layer reduces required laser power correspondingly, hence it is a strong driver for future visible wavelength LGS AO where the power requirements otherwise grow beyond what is feasible. These experiments are scheduled to take place early next year, after we receive a suitable laser.

Adaptive Optics Systems, edited by Norbert Hubin, Claire E. Max, Peter L. Wizinowich,
Proc. of SPIE Vol. 7015, 70150G, (2008)
0277-786X/08/$18 · doi: 10.1117/12.790228

Table 1. Summary of MEMS-AO / Villages Experiments

Phase	Experiment Description	Demonstrates	Impact
Phase 1			
Experiment 1	Closed loop on-sky demo using MEMS	MEMS will work for astronomical AO	Reduced risk for Keck and TMT AO
Experiment 2	Open loop on-sky demo using MEMS	MEMS will work in the MOAO architecture	MOAO architecture is feasible for Keck and TMT designs
Phase 2			
Experiment 3	Produce small LGS spot with Uplink AO	A small LGS spot can be produced; SNR increased	Choice of laser and launch facility for Keck, TMT
Experiment 4	Close the loop on the small spot LGS	Small LGS spot concept works	Visible λ AO system designs

The Villages system also functions as a general test bed for AO wavefront sensors and algorithms. We plan to modify the wavefront sensor into a pyramid-lenslet wavefront configuration this summer for testing to compare to predicted theoretical and laboratory performance. We also plan to test proposed wind estimation and predictive control algorithms

2. VILLAGES EXPERIMENTS

2.1 Optical Layout

The AO optical bench was designed to allow maximum flexibility in configuring Villages experiments. A schematic drawing showing beam paths appears in Figure 1. Light from the telescope first reflects off a fast tip/tilt mirror and is then split into two paths, one which is corrected by the DM and one which is not. The two beams allow simultaneous wavefront sensing of both pre and post-correction wavefronts and simultaneous imaging of far-field PSFs. The wavefront sensor camera CCD focal plane is divided into four regions two of which are assigned to Hartmann sensing of the pre and post corrected wavefronts. The other two regions are assigned to far-field tip/tilt sensing, and outgoing laser wavefront sensing. In the split path to the wavefront sensors and science camera, the first or second beam splitters can be removed or replaced with mirrors or dichroics, enabling a large number of observing modes. For example, removing the first splitter puts the system in conventional closed-loop configuration; removing the second splitter allows open-loop wavefront sensing and corrected imaging

A laser line transmitting dichroic at splitter one will allow imaging of the sharpened laser spot while wavefront sensing on a natural star. A laser line reflecting dichroic at splitter two will allow closed-loop laser guidestar wavefront sensing and corrected imaging of natural starlight. The bench mechanics and the telescope mounting system are designed to maximize mechanical stability, which is critical for diffraction limited visible wavelength work. A companion paper discusses details going into the engineering.[1]

2.2 Open and Closed Loop Wavefront Sensing and Control

Figure 2 shows the layout of the wavefront sensor. The first experiments with Villages were designed to demonstrate the feasibility of using MEMS deformable mirrors in a conventional closed loop AO arrangement. The Hartmann pattern in the upper right quadrant contains the residual wavefront information, after DM correction. The second set of Villages experiments are intended to demonstrate the feasibility of using MEMS in open-loop wavefront control. The Hartmann pattern in the lower right quadrant contains the open loop wavefront information, prior to DM correction. The Villages AO controller can be switched on demand from closed loop to open loop operation.

The open loop control requires that the DM be repeatable to nm accuracy given repeated voltage patterns, a trait that the MEMS DMs have shown quite well in the laboratory [2]. It is not then necessary that the DM be linear, but that it can be

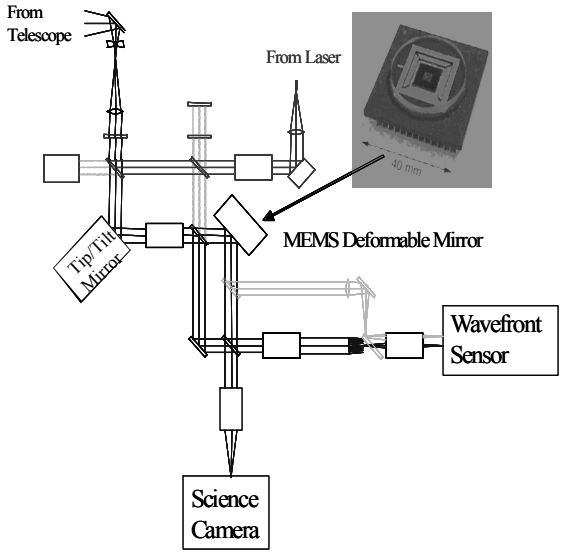

Figure 1. MEMS-AO / Villages system. The system employs a 140 actuator MEMS deformable mirror and fits on the back of the Lick Observatory 1-meter Nickel telescope.

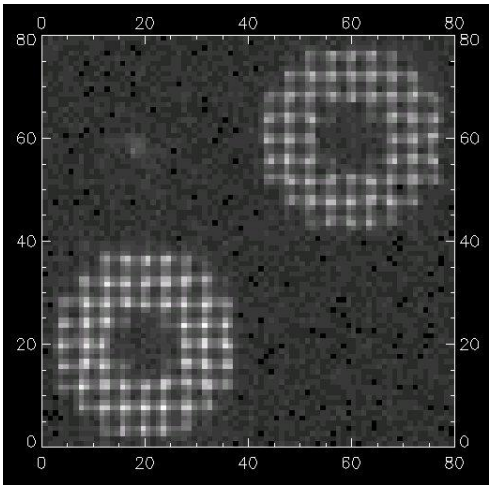

Figure 2. Wavefront Sensor layout. Upper right Hartmann pattern is the closed-loop, or residual wavefront as seen after the deformable mirror. The lower left pattern is of the open-loop, or prior to correction, wavefront. The upper left quadrant is the focal plane of the tip/tilt star sensor. The lower left quadrant is reserved for a future outgoing laser Hartmann sensor.

modeled accurately so that a real-time controller can repeatably derive the proper command voltages given a desired wavefront. It is also necessary that the wavefront sensor be linear over a high dynamic range, or calibrated so that suitably linearized measurements can be made.

2.3 Tip/Tilt Sensing

Laser guide star adaptive optics systems derive tip/tilt information from a natural star in the field. The field star is generally too dim for full wavefront sensing, hence the need for the laser, but is suitable for tip/tilt measurement at a focal plane. If the higher-order components of the tip/tilt star's wavefront are being adaptively corrected to fractions of a wave in the wavelength band at which it is being sensed, its image has a diffraction-limited core, albeit jumping around the focal plane at the atmospheric rate. This sharpened tip/tilt star appears much brighter and smaller (instantaneously) than a seeing-limited star, and hence is easier to guide on. The consequence is that very much dimmer natural guide stars can be used for tip/tilt sensing, which can significantly increase the fraction of the sky accessible for AO.

To get an idea of the improvement possible we use an approximate formula for tip/tilt centroiding error:

$$\sigma_{tt} = \frac{\lambda}{d}\frac{1}{\mathrm{SNR}} = \frac{\lambda}{d}\frac{\sqrt{N + B(\lambda/d)^2}}{N} \tag{1}$$

where N is the number of detected photons per frame, B is the sky background expressed as number of detected photons per frame per sterradian of sky, λ is the sensing wavelength, and d is the effective aperture size. We assume that centroiding occurs over an area comparable with the size of the spot on the detector, so as to minimize the effect of sky background noise. Solving (1) for N, the number of photons needed to achieve a given tip/tilt error, σ_{tt}, is given by

$$N = \frac{1}{2\sigma_{tt}^2}\left(\frac{\lambda}{d}\right)^2\left(1 + \sqrt{1 + 4B\sigma_{tt}^2}\right) \tag{2}$$

With AO sharpening of the star, the effective aperture is the diameter of the telescope ($d = D$), whereas, in uncorrected seeing the effective diameter is the seeing coherence length ($d = r_0$). Thus, for a given tip/tilt measurement accuracy, the number of photons required from a sharpened guide star is reduced by the factor $(D/r_0)^2$ over an uncorrected star. In the r_0=10 cm seeing at Mt Hamilton with a 1 meter telescope (Villages) this would be a factor of 100 increase in sensitivity, or 5 stellar magnitudes. For a 10 meter telescope on Mauna Kea in 20 cm seeing (Keck), the sensitivity increase is a factor of 2500, or 8.5 stellar magnitudes.

According to published star-density models [3][4] a 5 magnitude improvement in sensitivity can mean roughly a factor of 10 increase in the number of available guide stars. In V band, the isokinetic angle on Mt Hamilton is about 10 arcseconds (essentially independent of telescope size, but strongly dependent on seeing), where we have defined the isokinetic angle as the separation angle at which rms tip/tilt differs by the diffraction limited full-width-half-max. On Mauna Kea, with the better seeing, the isokinetic angle is about 20 arcseconds. AO systems today require a 16th magnitude or brighter tip/tilt star to obtain reasonable Strehl performance. As we move toward visible band AO, the required brightness will only increase. The average on-sky chance of finding a J magnitude 16 tip/tilt star in a 40 arcsecond diameter V band isokinetic neighborhood is about 20% (Spagna model) whereas the coverage for J=21 tip/tilt stars is about 80%. For visible wavelength AO systems, sharpening the tip/tilt star is thus essential to attaining reasonable sky coverage.

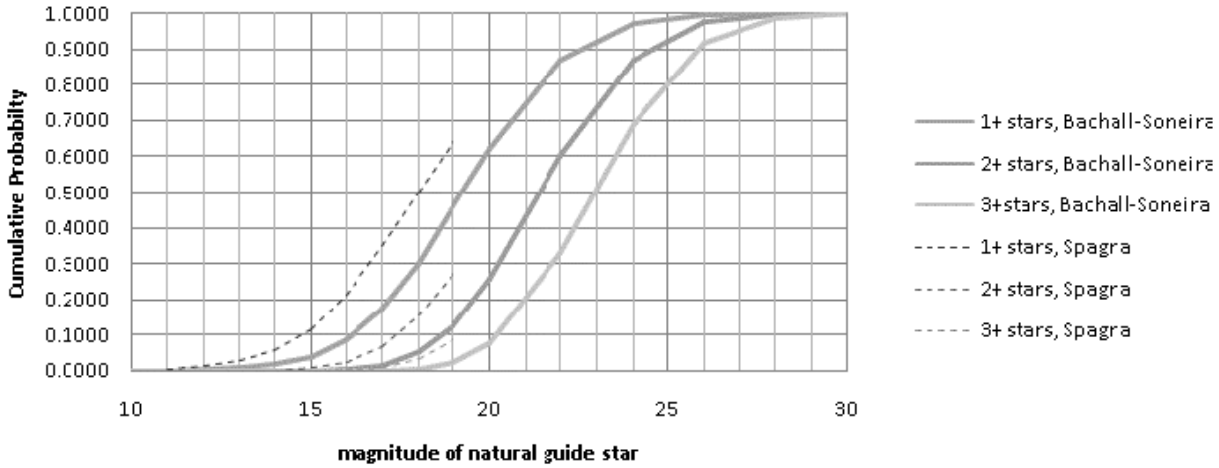

Figure 3. Probability of finding > 1,2, or 3 tip/tilt stars within the V band isoplanatic patch as a function of star magnitude, assuming the Bachall-Soneira model for stars sensed in the V band and the Spagna model for stars sensed in the J band. Current AO systems use V=16-18 guidestars. AO sharpening will improve this limit (for a 10 m telescopes) to V=24, where there's a good chance of a star being in the isokinetic angle. Curves shown are for the sky at 30 degrees galactic latitude. Two and three star case are shown because visible wavelength AO systems on large aperture telescopes will need to have multiple laser guidestars to reduce cone effect and mitigating the unsensed LGS tip/tilt modes will require more than one natural tip/tilt star.

According to the models (Figure 3), star abundance is less in V than in J band at a given magnitude, i.e. infrared stars are more plentiful on the sky. The net effect is that at a given star density J band stars are brighter by about a magnitude. However, the diffraction limit in V is smaller by a factor of 2 than in J so, even though photon flux counts in V and J bands for a given magnitude star are roughly equal, the smaller size provides more than a factor of 4 increase in sensitivity (even more, because the sky background flux is higher in J than V) and this more than overcomes the star brightness difference at a given density. So, for a V band correcting AO system, sensing tip/tilt stars in V is more efficient than in J. The only advantage to using J band would be if the (high-order wavefront) Strehl ratio is better in J than in V by a factor of 4. For Villages, the high-order wavefront contribution to Strehl is expected to be about 0.3, thus sensing tip/tilt in V band is more efficient, with the added benefit of being less costly since we can use a portion of the wavefront sensor CCD for this purpose rather than a separate IR array.

From equation (2) we can see that the presence of sky background does not affect the conclusion that sharpening the star improves sensitivity by a factor of $(D/r_0)^2$. Background starts to have significance to the required signal flux when its integrated flux over the desired rms tip/tilt blur is on the order one photon per frame time. Sky brightness at Mauna Kea

is less than 1 photon/s/m^2/nm in V band and 100 photons/s/m^2/nm in J band [5]. Assuming desired rms tip/tilt blur is on the order of the diffraction limit, it is useful to express sky background in terms of magnitude per square diffraction-limit. For a 10 meter aperture diffraction limit, this works out to a V band brightness of magnitude 30 and a J band brightness of magnitude 25.5 per diffraction limit. Tip/tilt stars brighter than this will always be photon-limited since they are brighter than the sky at the diffraction limit. For the 1 meter Village aperture and the somewhat brighter sky background at Lick, these magnitudes are V=24 and J=19. Thus, even though sensors for sharpened tip/tilt stars will be operating closer to the sky background limit, they will still most likely be running in the photon-limited regime.

2.4 Laser Uplink Correction

The Villages system is set up for shared-aperture laser launch, that is, the laser will be projected from the 1m telescope aperture. The intent is to produce a smaller laser guide star spot in the mesosphere by applying AO wavefront control to the outgoing laser beam. The upgoing laser wavefront is pre-corrected with the opposite of the atmospheric aberrations to be seen along its path. The beam will then emerge from the upper atmosphere diffraction-limited and go on to form a diffraction-limited spot at the sodium layer.

The choice of projection aperture for an uplink-corrected laser is optimized by balancing diffraction width against geometric width of a focusing beam as within the finite thickness of the sodium layer. Assuming that we wish to capture return photons coming from all altitudes in the sodium layer, we choose a launch aperture size that has a depth of focus equal to the sodium layer thickness:

$$\delta z = 2\left(\frac{z_{Na}}{D_p}\right)^2 \lambda \qquad (3)$$

where z_{Na}/D_p is the effective f/number of the beam converging at the altitude of the sodium layer and δz is its thickness. For λ = 589 nm, z_{Na} = 90 km, δz = 10 km, the aperture size is D_p = 1 meter. The size of the spot at the sodium layer is $z_{Na}\,\lambda/D_p$ = 10 cm, or approximately 0.2 arcseconds of subtended angle. This is approximately 10 times smaller than the smallest LGS spot reported so far (as to be expected from the improvement over seeing limited propagation). With such a small spot there is a potential for much greater efficiency in wavefront sensing. In particular, our recent simulations of a diffractive pyramid sensor have shown that beacon photon flux could be reduced by a factor of 100 over Hartmann sensors and still achieve diffraction-limited wavefront measurement[6].

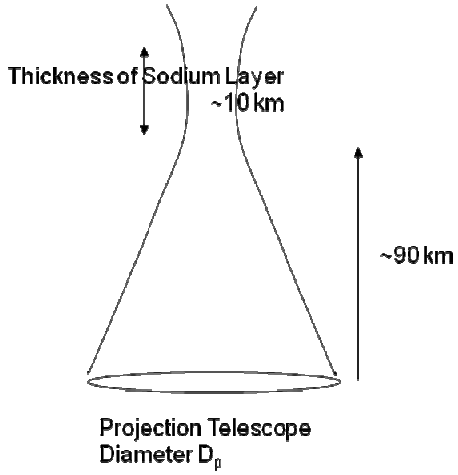

Figure 4. Geometry of the uplink laser beam focusing on the sodium layer. Depth of focus equals sodium layer thickness, producing the smallest subtence as seen from the ground..

The Hartmann sensor is not the right choice because the subaperture lenslets blur the spot due to diffraction. Hartmann sensors are designed with $d = r_0$ at the science wavelength in order to critically sample the wavefront, thus the Hartmann spots are essentially seeing-limited and a guidestar projection from a telescope aperture of diameter $D_p > r_0$ is of marginal benefit.

There have been a number of atmospheric wavefront sensing concepts described in the literature which are rooted in exploiting the diffractive properties of the light. These schemes have two advantages: 1) they do not break up the wavefront into small subapertures, thus the spatial coherence properties of the source are preserved, 2) direct optical phase sensing eliminates a troublesome noise amplification factor inherent in slope to phase reconstruction algorithms. These methods include the point diffraction or Smartt interferometer [7], the curvature sensor with wave-optic reconstructor [8], and the diffractive pyramid sensor [9][10]. Although curvature and pyramid sensors have been in use in AO systems for some time, the full advantage of direct phase sensing is yet to be demonstrated on sky.

We plan to install a diffractive pyramid wavefront sensor (PWFS) in the Villages experiment later this year. This sensor is based on using a microlenslet array in the focal plane [11]. The light is focused at the junction of four lenslets. The lenslets then form four pupil images onto a CCD detector plane which is sampled across the pupil at one pixel per r_0. The microlenslet array has several advantages. 1) the lenslets themselves are precisely manufactured so as to have nearly

defect-free boundaries with neighboring lenslets; this minimizes the loss of light due to edge defects; 2) the positive optical power of the lenslet reimages the pupil, removing the need for an additional collimator lens; 3) the lenslet's size acts naturally as a field stop. If properly chosen with respect to the f/# of the beam, the lenslet can function as a spatial filter, which reduces wavefront sensor aliasing error [12].

With an uplink corrected laser and a direct phase wavefront sensor, we can expect the laser power requirement to decrease drastically. Essentially we need only one detected photon per frame per r_0 to measure the wavefront to the diffraction limit [6]. However, there is an important limitation: we must not allow the detected photons per frame per r_0 to drop below the detector read noise. The best detector is one with zero read noise. Our current 5-6 electron read noise per pixel detectors actually defeat the advantage of the small guide star spot and direct phase sensing when the practical details of uplink Strehl ratio and sensor losses are taken into account. Table 2 shows a performance comparison at conditions relevant to Villages. With zero noise detectors, visible wavelength LGS adaptive optics, with a Strehl of 0.3 at 600 nm, is possible with *one to two Watts* of laser power.

	Pyramid WFS, Uplink AO Correction				Hartmann WFS, No Uplink AO	
Laser Power	1W	2W	3W	4W	10W	50W
Detector Read Noise Electrons 0	44	29	23	35	25	8
1	58	38	30	36	26	8
2	xxx	52	39	39	28	9
3		xxx	57	42	31	9
4			xxx	102	31	17
5				xxx	33	18
6					35	19

Table 2. Simulated comparisons of wavefront measurement error for various laser powers and levels of detector read noise. Errors are given in nanometers rms. Conditions are wind blown turbulence at r_0=11 cm and a wind speed of 5 m/s, typical of good seeing on Mt Hamilton. The calculations take into account a number of practical efficiency and throughput numbers emulating the Villages system conditions, including consideration of pyramid sensor diffraction losses and Strehl of the uplink beam correction. X's indicate the boundary of practical direct phase wavefront sensing, where the signal photons drop below the read noise per pixel.

The advantages of uplink AO and direct phase sensing could have a tremendous impact on the design of future visible wavelength AO systems. Unless 589 nm laser power suddenly becomes a lot cheaper, it may be the only way to make multiple laser guidestar visible AO feasible.

On the Villages AO bench, provision is made for merging the laser into the telescope beam path using a polarization beam splitter. With the laser linearly polarized, almost all of the power is launched, and if the light comes back in a random polarization, approximately ½ the laser return light can go into the receiver (then further split or selected between wavefront sensor and science camera). The uplink correction is performed on the AO bench using a second deformable mirror. This DM will need to be coated to withstand the heat load from the laser pulse. The uplink mirror selection is yet to be finalized, but there are a number of viable candidates. The control of the uplink DM is equivalent (by Fermat's principal) to that of the receiver DM, thus both mirror controls are derived from the wavefront sensor sensing the downlink beam.

2.5 Laser Format

The sodium guidestar return in photons per projected Watt is quite dependent on the spectrum and pulse format of the laser. Obviously one wants to make the return efficiency as high as possible. Within the last few years, work at the Starfire Optical Range has led to the development of a narrow band (10kHz) CW laser that has achieved very high return efficiency in on-sky experiments, the best reported so far [13]. Theoretical analysis has explained the result: a narrow CW line addresses only one Doppler class of the sodium atoms with a single wavelength and does not suffer from a quenching effect that that happens when a broader line addresses multiple classes all with a range of wavelengths [14][15][16]. Lasers on current astronomical AO systems use various pulse formats none of which have had the same return performance as the narrow band CW, although one, the laser at Palomar, has been tuned to a reasonably good multi-line format and is now achieving improved return but not as high as the CW one [17].

Unfortunately, a CW laser is not the optimum format for AO system design. It is more desirable to use a pulsed laser for two reasons: 1) laser pulse tracking through the sodium layer so as to remove LGS spot elongation (important on large telescope apertures), and 2) avoiding Rayleigh backscatter by gating the wavefront sensor only after the pulse is above most of the atmosphere. For reason 1, the optimum pulse length is about 3 microseconds. For reason 2, the optimum pulse rate is about 3 kHz (this puts 2 pulses in the air at any given time, separated by enough distance to gate out the first 30 km of atmospheric backscatter. Example pulse diagrams are shown in Figure 5. If the laser is narrowband single frequency, or spectrally formatted so that laser lines are separated by more than 150 MHz (so that they address independent Doppler bins without quenching cross-excitation), then long 3 microsecond pulses are in theory tolerable. Transform broadening is less than 1 MHz, which stays well within a single Doppler class of 30 MHz bandwidth, set by the 27 ns decay time of the sodium D2 transition. However, we have yet to demonstrate an on-the-sky pulsed laser having the same sodium return efficiency as the SOR CW laser.

The Center for Adaptive Optics (CfAO) and the Adaptive Optics Development Program (AODP) have been funding the development of an experimental fiber laser at the Lawrence Livermore National Laboratory (LLNL). This laser (described in a companion paper) is inherently CW but can be tuned both in spectral and pulse format using electro-optic modulators, leading to an interesting set of experiments with the Villages system. The laser will be spectrally formatted with about 9 narrow lines evenly positioned within the 2 GHz Doppler broadened sodium D2 line and will initially be set up with a pulse format suitable for Rayleigh blanking. Rayleigh blanking in the Villages experiment is essential, since the Nickel telescope primary is shared as both the projection and the receiving aperture. A chopper wheel on the Villages optical bench gates the received pulses. Current plans are to complete the laser this summer, thoroughly test in the lab over the winter, and install on the Nickel in summer 2009 for on sky experiments.

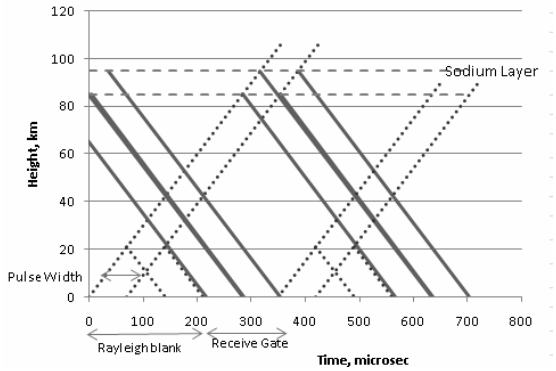

Zenith Angle, degrees	Pulse Width, microsec	Rep Rate, kHz
0	70	2.8
20	75	2.67
30	82	2.4
45	100	2

Figure 5. Laser Pulse formats. Left: A Rayleigh blanking format with a 70 microsec pulse, where two pulses are in the air at once. Dotted lines indicate the tip and tail of an upgoing pulse, and its Rayleigh backscatter. Solid lines indicate the return signal, stretched by the transition time through the sodium layer. The receive gate must be open for 137 microsec. Since the distance to the sodium layer varies with zenith angle, we need to arrange for a number of different pulse formats to cover the range of pointing angles. The table on the right shows the variations chosen. One of the practical considerations is to keep the duty cycle > 20% which is a good operating point for fiber laser performance.

The Villages laser experiments will consist of two components: experiment 1) measure the size and photometric return properties of the laser/laser uplink system; experiment 2) perform closed loop LGS operation. With the Villages setup we can close the loop using a bright natural guidestar and then image the sodium guidestar in the science camera. This will enable us to view the spot at enough resolution to detect sharpening, without having to rely on closing an LGS loop.

Experiment 2 is speculative, and might require a component we don't have yet, a 0-2 electron read noise WFS camera. Should the laser produce 10 Watts and attain the CW return efficiency, we should be able to close the LGS loop with our existing camera and no uplink AO. With a 0-2 e- read noise camera, *only a watt or two* output from this laser should be enough to close an LGS AO loop and correct stars in the visible. This is assuming all goes well with uplink correction and the pyramid wavefront sensor, and that the laser produces CW return efficiency.

2.6 Pulse Tracking

On large aperture telescopes, there is considerable elongation of the Hartmann image of a laser guide star in subapertures separated some distance from the laser projector, caused by off-axis viewing of the beam through the finite thickness of the sodium layer. The effect is to reduce centroiding accuracy because of the spreading out of light on the detector. The

real issue is that the larger aperture telescopes reimages different altitudes of the sodium layer at different back focal distances so the light rays fill a region deeper than the telescope depth of focus and wider than the beam image from any single altitude. With a short laser pulse (3 microseconds) and rapid mechanical defocusing ahead of the LGS focus, the laser light can be piled back in to the depth of focus. This eliminates elongation in the Hartmann sensor, and also, importantly, enables direct phase sensing since the small spot size is restored.

The Villages receiving aperture, the 1 meter Nickel telescope, is not large enough for LGS elongation to be a concern, even if the LGS spot is diffraction-limited (the depth of focus of the 1 meter telescope is the thickness of the sodium layer, as calculated using equation (3)). Therefore we have no plans to experiment with pulse tracking using the Villages system, although we are considering experimenting with a variable focus element in the laboratory.

3. FIRST LIGHT RESULTS

The first on-sky closed loop experiments with bright natural guide stars were performed in November, 2007. In this run we were able to achieve up to 25% Strehl ratio at 900 nm imaging wavelength (169 nm rms residual wavefront error). The image and chart in Figure 6 show some of the Strehl performance results. Our ultimate goal for the system is a closed-loop Strehl of 0.3 in V band (87 nm rms residual wavefront error) under "ordinary" (r_0=11 cm, v_{wind} = 5 m/s) seeing conditions which we should reach later in the season this year. The MEMS device worked flawlessly and met our Experiment 1 goals of demonstrating MEMS suitability and robustness for astronomical AO in observatory conditions.

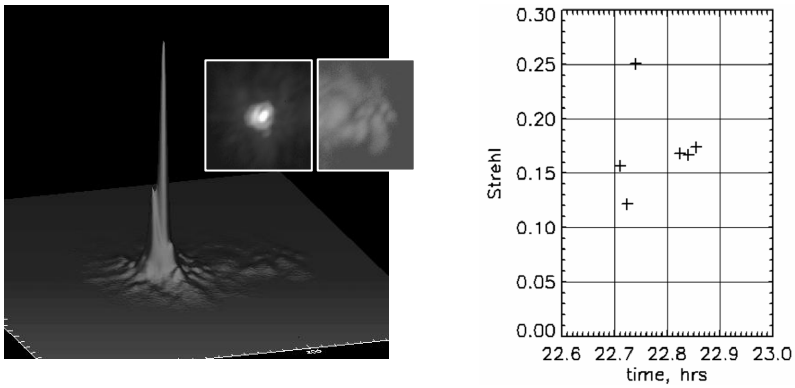

Figure 6. Left: Simultaneous images of DM corrected and uncorrected star α-Ari in I band (λ=0.9 μm) from observations on 11/21/07. Surface plot is linear scale. Inset images are log-stretched grey scale, with the corrected image on the left and the simultaneous uncorrected image on the right. Right: Strehl ratio over several short exposure (50 msec) images of α-Ari in I band.

The first on-sky open loop control tests were performed in early 2008. Figure 7 shows representative PSFs. The system achieved the diffraction limit in I (800 nm) and R (650 nm) bands, but not in V (550 nm), although in V the PSF was tighter and rounder than open seeing and had a full width half max of a little less than one half arcsecond.

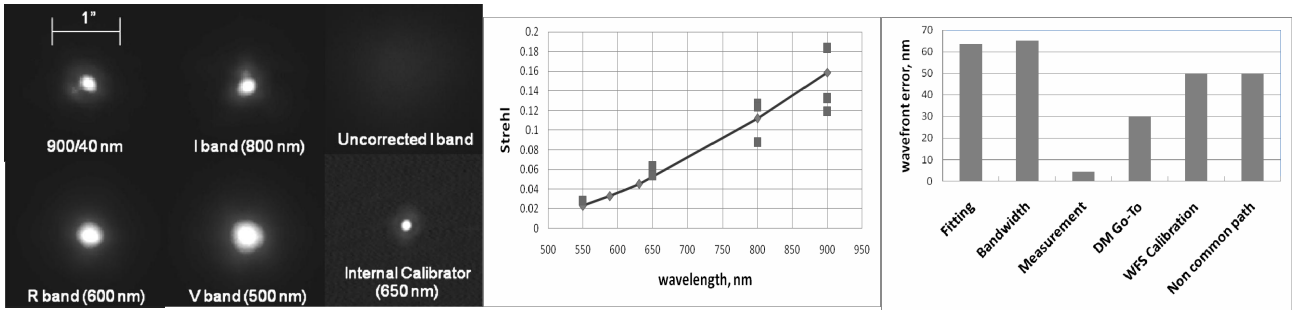

Figure 7. Left: PSFs with open-loop control, from observations on 4/16/08. Middle: Measured Strehls and a representative error budget model fit. Right: Error budget allocation that it is consistent with independent measurements of r_0=7cm, wind=14m/s, and internal errors. DM go-to error was measured in an interferometer to 15 nm surface [2], WFS calibration error is based on wave-optic simulation and analysis of our wavefront sensor, and non-common path error is determined by measuring the Strehl on an internal diffraction-limited reference source.

Considerable telemetry data is available from the real-time system. This data includes WFS camera frames, computed Hartmann centroids, reconstructed wavefronts, DM mirror voltages, tip/tilt sensor readings, and tip/tilt mirror commands. Analysis of this data allows us to characterize compare the open and closed loop performance of the AO controller vs both spatial and temporal frequency.

Figure 8 shows temporal power spectra of corrected high-order wavefronts collected on a bright star at a WFS frame rate of 750 Hz. Since the system senses between both pre and post correction wavefronts simultaneously, the data on each graph are over the same atmospheric realizations. The closed loop disturbance rejection (ratio of corrected to uncorrected wavefront) shows the classic single integrator feedback behavior, where rejection at low frequencies goes as f^{-1}. The crossover frequency (frequency at which the disturbance rejection ratio crosses 1) is about 30 Hz. The open loop control disturbance rejection also shows a region of f^{-1} rejection behavior, but flattens out at the lowest frequencies to a minimum level of about 0.02. The open loop control crossover frequency is much higher than for closed loop, about 200 Hz. Open loop control relies on accurate high dynamic range wavefront sensing to measure the uncorrected wavefront and an accurate open loop model of the deformable mirror to control it in one step to correct the measured wavefront. With a control gain of unity on each cycle, its temporal frequency response is much better (crossover at 200 Hz). The closed loop control law (crossover at 30 Hz) has to use a smaller control gain (about 0.1 per cycle) in order for the feedback loop to remain stable, however any persistent residual error on the DM eventually converges to zero as it is repeatedly measured and compensated. In the open-loop case the sensor does not see any residual DM error so the lower limit to low frequency rejection reflects error in the open loop modeling (combined WFS linearity and DM go-to model). The 2% error evident here is consistent with the care we have taken in calibrating the wavefront sensor and tuning the DM open loop model.

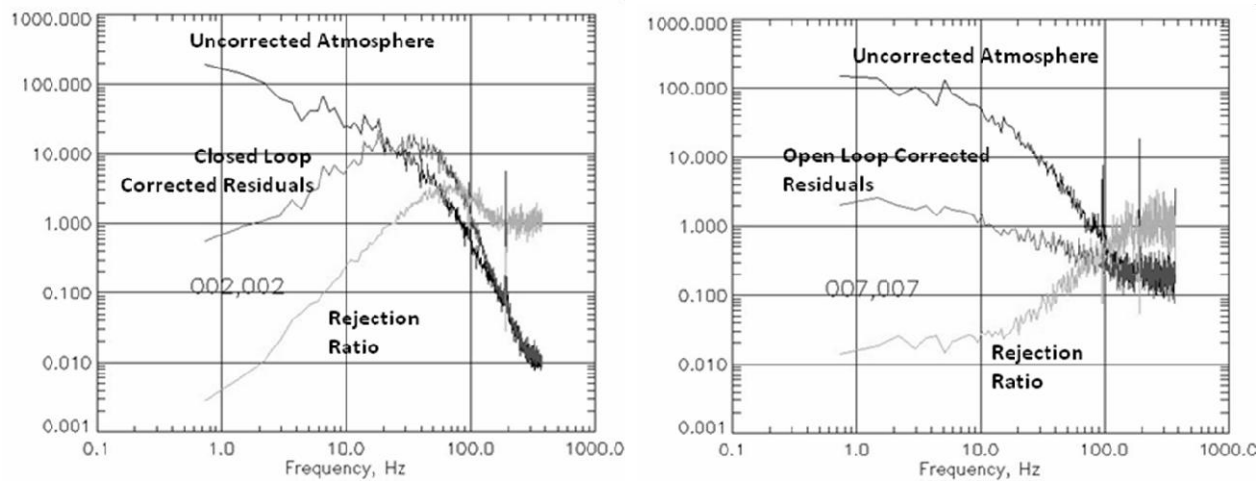

Figure 8. Temporal power spectra of rms reconstructed wavefronts, representing 1.4 seconds of 750 Hz data from the wavefront sensors. The left panel shows the closed loop control spectra and the right panel shows the open loop control spectra. Lighter curves are the ratio of corrected to uncorrected spectra, exhibiting the characteristic controller rejection behavior described in the text.

By monitoring the change in the low frequency rejection ratio of open loop control over the course of the year, we can monitor any drifts in our calibration of the open loop model. We continue to use the same DM open loop control model (a combination of linear plate equation theory with empirical nonlinear actuator fits) determined in the lab with an interferometer almost a year ago. So far we have seen perhaps a slight drift, up to closer to 5-6% error, but since this can be due to a number of systematic error sources including alignment it is currently work in progress to determine whether this is significant.

The wavefront sensor uses 4x4 pixel Hartmann subapertures, with each pixel subtending about 2 arcseconds of sky. There is a field stop at the focus in front of the sensor that passes an 8 arcsecond diameter field so as to prevent cross-talk amongst the subapertures. The pixel sampling results in a reasonably linear measurement of spot displacement if a center of mass centroider is used. The nonlinearity error is calculated to be about 50 nm rms contribution to overall wavefront. Other Hartmann centroiding algorithm, such as for example quad cell, matched filter, least squares, etc. do not perform well in open loop control, since they are significantly more nonlinear over the uncorrected dynamic range.

An interesting feature visible in all the temporal power spectra is a pair of spikes at close to 100 and 200 Hz. The problem is quite evident in the tip/tilt data (Figure 9). We chased this down to wind buffeting exciting a structural resonance in the cassegrain mounting system of the Villages optical bench. Unfortunately this resonant frequency and its harmonic are outside the bandwidth of our tip/tilt system. The peak-to-valley excursions of 0.1 arcsecond are a significant source of Strehl loss especially at the shorter wavelengths (this vibration was included in the error budget model presented in Figure 7). We've added some dampening material to the mounting struts try to suppress this vibration, which seems to have a reasonably mitigating effect most of the time, but it is still not at a desirable level.

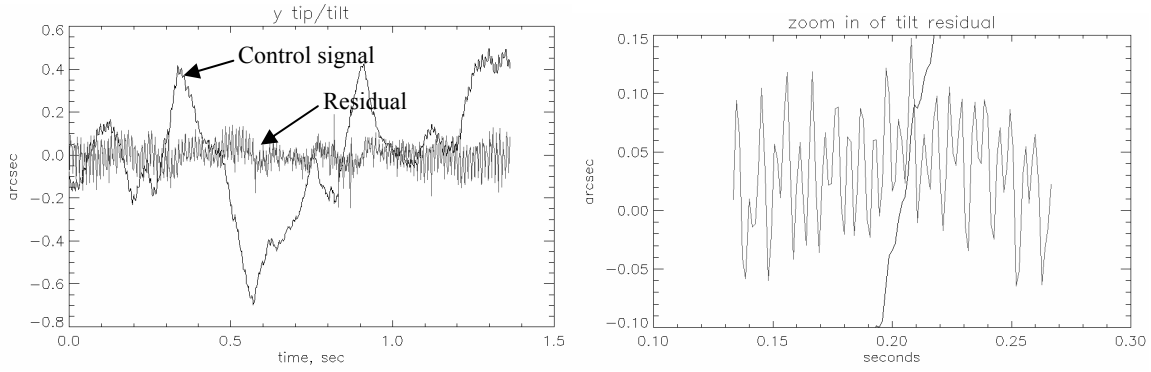

Figure 9. Structural vibration evident in the tip/tilt data. The 0.1 arcsecond excursions are a significant cause of Strehl loss in V band, so we have taken steps to try to suppress the resonance. The amplitude is highly correlated to the wind speed over the dome slit.

4. CONCLUSIONS

The Villages experiment is the on-sky platform for testing advanced AO concepts developed at the Laboratory for Adaptive Optics. The long-term goal is to prove out the technologies that will enable feasible and cost-effective laser guide star (high sky coverage) adaptive optics astronomy in the visible wavelength bands. It also functions as a risk-reduction testbed for intermediate stages of technology development that are critical to proposed new "next generation" AO instruments for Keck and TMT. We have had a successful set of observation runs that have demonstrated the use of MEMS deformable mirrors and have shown that they can be operated in closed loop without any measureable Strehl loss. We will continue to perform experiments and monitor the system performance as seeing gets better during the year, looking for discriminators of drift, calibration, or implementation errors in open loop control. Next year's plans include experiments with laser guidestar uplink AO.

ACKNOWLEDGMENTS

The Villages experiment was supported through a Small Grant for Exploratory Research from the Astronomy Division of the National Science Foundation, award number 0649261. Further support was provided from the UCO/Lick Observatory and from a generous grant provided by the Gordon and Betty Moore Foundation to UCO/Lick to establish the Laboratory for Adaptive Optics.

REFERENCES

[1] B. Grigsby, C. Lockwood, B. Baumann, D. Gavel, J. Johnson, S.M. Ammons, D. Dillon, K Morzinski, M. Reinig, D. Palmer, S. Serverson, E. Gates, "ViLLaGEs: Opto-Mechanical Design of an on-sky visible-light MEMS-based AO system," SPIE 7015 (2008).

[2] K. Morzinski, D. Gavel, A. Norton, D. Dillon, M. Reinig, **"**Characterizing MEMS deformable mirrors for open-loop operation: high-resolution measurements of thin-plate behavior**,"** SPIE, 6888, 68880S-68880S-12 (2008).

[3] J. Bahcall and R. Soneira, "The Universe at Faint Magnitudes. I. Models for the Galaxy and the Predicted Star Counts," Astrophysical Journal Supplement, 44:73-110, (1981).

[4] A. Spagna, "Guide Star Requirements for NGST: Deep NIR Starcounts and Guide Star Catalogs," STScI-NGST-R-0013B, (2001).
[5] A. Bouchez, "Keck Next Generation Adaptive Optics Background and Transmission Budgets," Keck Adaptive Optics Note 501, (2007).
[6] R. Kupke, D. Gavel, J. Johnson, M. Reinig, "Implementation of the pyramid wavefront sensor as a direct phase detector for large amplitude aberrations," SPIE 7015 (2008).
[7] J. Codona and R. Angel, "Imaging Extrasolar Planets by Stellar Halo Suppression in Separately Corrected Color Bands," Astrophysical Journal Letters, 604, L117, (2004).
[8] Guyon, O., Blain, C., Takami, H., Hayano, Y., Hattori, M., Watanabe, M., "Improving the Sensitivity of Astronomical Curvature Wavefront Sensor Using Dual-Stroke Curvature," PASP, Volume 120, issue 868, pp.655-664, (2008).
[9] Verinaud, C., "On the nature of the measurements provided by a pyramid wavefront sensor, " Opt. Comm., **233**, 27-38 (2004).
[10] Johnson, J. A., Kupke, R., Gavel, D., and Bauman, B., "Pyramid wavefront sensing: Theory and component technology development at the LAO," in *Advances in Adaptive Optics II,* B. Ellerbroek and D. Bonaccini, eds., Proc SPIE **6272** (2006).
[11] B. Bauman, "Optical Design for Extremely Large Telescope Adaptive Optics Systems," PhD Thesis, University of Arizona, (2003).
[12] L. Poyneer and B. Macintosh, "Spatially filtered wave-front sensor for high-order adaptive optics,", J. Opt. Soc. Am. A/Vol. 21, No. 5, (2004).
[13] C. Denman, J. Drummond, M. Eickhoff, R.Q. Fugate, P. Hillman, S. Novotny, J. Telle, "Characteristics of sodium guidestars created by the 50-watt FASOR and first closed-loop AO results at the Starfire Optical Range," SPIE 6272, (2006).
[14] J. Telle, J. Drummond, P. Hillman, C. Denman, "Simulations of mesospheric sodium guidestar radiance," SPIE 6878, (2008).
[15] P. Hillman, "Effects of Atomic Recoil on Photon Return using a CW Single Frequency FASOR," Presented at the 2007 CfAO Fall Workshop on Laser Technology and Systems for Astronomy, (2007).
[16] P. Hillman, "Sodium Guidestar Return From Broad CW Sources," Presented at the 2007 CfAO Spring Workshop on Laser Technology and Systems for Astronomy, (2007).
[17] V. Velur, E. Kibblewhite, R. Dekany, M. Troy, H. Petrie, R. Thicksten, G. Brack, T. Trin, M. Cheselka, "Implementation of the Chicago sum frequency laser at Palomar laser guide star test bed," SPIE 5490, (2004).